Predictive potential of Perzyna viscoplastic modelling for granular geomaterials

Lazari, Maria; Sanavia, Lorenzo; di Prisco, Claudio; Pisanò, Federico

DOI
10.1002/nag.2876

Publication date
2018

Document Version
Accepted author manuscript

Published in
International Journal for Numerical and Analytical Methods in Geomechanics

Citation (APA)
Lazari, M., Sanavia, L., di Prisco, C., & Pisanò, F. (2018). Predictive potential of Perzyna viscoplastic modelling for granular geomaterials. *International Journal for Numerical and Analytical Methods in Geomechanics*, *43 (2019)*(2), 544-567. https://doi.org/10.1002/nag.2876

Predictive potential of Perzyna viscoplastic modelling for granular geomaterials

M. Lazari [a, *], L. Sanavia [a], C. di Prisco [b] and F. Pisanò [c]

[a] Department of Civil, Environmental and Architectural Engineering, University of Padova, Padova, Italy
[b] Department of Civil and Environmental Engineering, Politecnico di Milano, Milan, Italy
[c] Faculty of Civil Engineering and Geosciences, Delft University of Technology, Delft, Netherlands

[*] Corresponding author.
E-mail address: lazari.maria1@gmail.com

ABSTRACT

This paper reappraises Perzyna-type viscoplasticity for the constitutive modelling of granular geomaterials, with emphasis on the simulation of rate/time effects of different magnitude. An existing elasto-plastic model for sands is first recast into a Perzyna viscoplastic formulation, then calibrated/validated against laboratory test results on Hostun sand from the literature. Notable model features include (i) enhanced definition of the viscous nucleus function, and (ii) void ratio dependence of stiffness and viscous parameters, to model the pycnotropic behaviour of granular materials with a single set of parameters, uniquely identified against standard creep and triaxial test results. The comparison between experimental data and numerical simulations points out the predicative capability of the developed model and the complexity of defining a unique viscous nucleus function to capture sand behaviour under different loading/initial/boundary and drainage conditions. It is concluded that the unified viscoplastic simulation of both drained and undrained response is particularly challenging within Perzyna's framework and opens to future research in the area. The discussion presented is relevant, for instance, to the simulation of multi-phase strain localisation phenomena, such as those associated to slope stability problems in variably saturated soils.

Keywords: sand, creep, constitutive modelling, Perzyna viscoplasticity, strain localisation, regularisation

1 INTRODUCTION

There is wide experimental evidence of granular geomaterials responding to external perturbations rapidly but not instantaneously. The microstructural rearrangements that cause macroscopic deformations take place over time frames sometimes in the order of minutes – such as in the case of loose sands [1]. Laboratory investigations regarding strain rate effects, creep and relaxation in sand have been presented in [1]–[8]. In light of those experimental observations, the mathematical modelling of

granular soil behaviour may be successfully tackled in the framework of delayed plasticity theories – also referred to as viscoplasticity – or through a viscous evanescent relationship. Most viscoplastic models are formulated according to either of two different approaches: those allowing the stress state to lie outside the assumed elastic domain [9], [10] and those relying on rate-dependent hardening rules (consistency viscoplasticity, [11]–[14]). Alternatively, [15]-[16] proposed a viscous evanescent relationship within a general three-component model framework. Here, the former approach in the version proposed by Perzyna [9], [17] will be followed due to its proven capability to reproduce the rate-dependence of both fine- and coarse-grained soils [18]–[21], including creep and relaxation phenomena. Importantly, Perzyna's viscoplasticity has also proven a suitable conceptual platform for the interpretation of several soil instabilities ([19], [22]–[25]).

Viscoplasticity has also gained further success over the years as a regularisation technique for strain localisation simulations. This notable property relates to the intrinsic characteristic length possessed by viscoplastic media as a consequence of their time-sensitiveness ([11], [22], [26]–[30]). As a consequence, the ill-posedness of inviscid elasto-plastic problems at the onset of bifurcation can be remedied [31], as well as the pathologic mesh-dependence of corresponding finite element simulation results. Enhanced regularisation performance has also been achieved via a non-local reformulation of standard viscoplastic constitutive equations (e.g. [32], [33]). Such approach is beneficial for materials whose viscosity-related characteristic length is physically inaccurate, or in fact too small to produce any regularisation.

This work addresses the less investigated problem of formulating/calibrating viscoplastic models that can quantitatively capture the rate-dependent behaviour of sands under diverse loading/initial/boundary conditions. For this purpose, the existing elasto-plastic sand model by Buscarnera and Nova [34] (based on the previous work of Jommi [35], Jommi and di Prisco [36] and Nova et al. [37]) is reformulated according to Perzyna's viscoplastic approach and validated against experimental data from the literature. Special attention is devoted to the importance of the viscous nucleus definition – main factor affecting the rate-sensitiveness – and to the intrinsic pycnotropy of sand behaviour (dependence on the void ratio). The latter aspect is addressed by introducing a straightforward void-ratio dependence of certain soil parameters (viscosity, stiffness and hardening coefficients), as already explored e.g. by [38].

The ultimate goal of the work is to re-open a discussion on the fundamental requisites of viscoplastic sand models, not solely in terms of their regularisation performance, but primarily of their physical soundness predictive capability.

2 CONSTITUTIVE FORMULATION

The proposed elasto-viscoplastic model is formulated hereafter under the assumption of isotropic hydro-mechanical behaviour, also including the effects of variation in suction and/or degree of saturation for generality. The model builds upon the isotropic hardening formulation for unsaturated soils proposed in [34], based on the previous work of [35]−[37]. Direct notation is adopted, with boldface and lightface italic symbols denoting tensors/vectors and scalars, respectively.

2.1 Stress/strain variables and elastic law

The small-strain multiaxial formulation of the model is based on the following definition of the generalised effective Cauchy stress tensor $\boldsymbol{\sigma}'$ [39], applicable to three-phase porous materials with incompressible solid grains:

$$\boldsymbol{\sigma}' = \boldsymbol{\sigma} - S_{\mathrm{w}}\, p^{\mathrm{w}}\, \mathbf{1} - \left(1 - S_{\mathrm{w}}\right) p^{\mathrm{g}}\, \mathbf{1} \tag{1}$$

where $\boldsymbol{\sigma}$ is the total Cauchy stress tensor, p^w and p^g the pressures of pore liquid water and gas, S_w the water degree of saturation, and $\mathbf{1}$ the second-order identity tensor. The cases of dry and water saturated soil are recovered by setting S_w= 0 and S_w= 1, respectively.

The total strain rate is decomposed additively into elastic/reversible ($\dot{\boldsymbol{\varepsilon}}^{\mathrm{e}}$) and viscoplastic/irreversible ($\dot{\boldsymbol{\varepsilon}}^{\mathrm{vp}}$) components:

$$\dot{\boldsymbol{\varepsilon}} = \dot{\boldsymbol{\varepsilon}}^{\mathrm{e}} + \dot{\boldsymbol{\varepsilon}}^{\mathrm{vp}} \tag{2}$$

with the latter being by definition time-delayed. The elastic behaviour of the material emerges directly from a strain energy function $\psi\left(\boldsymbol{\varepsilon}^{\mathrm{e}}\right)$:

$$\boldsymbol{\sigma}' = \frac{\partial \psi}{\partial \boldsymbol{\varepsilon}^{\mathrm{e}}}\left(\boldsymbol{\varepsilon}^{\mathrm{e}}\right) \tag{3}$$

and can be than cast into the following rate form:

$$\dot{\boldsymbol{\sigma}}' = \mathbf{D}^{\mathrm{e}}\left[\dot{\boldsymbol{\varepsilon}} - \dot{\boldsymbol{\varepsilon}}^{\mathrm{vp}}\right] \tag{4}$$

In Equation (4) $\mathbf{D}^{\mathrm{e}}$ is the fourth-order elastic stiffness tensor given by:

$$\mathbf{D}^{\mathrm{e}} = \frac{\partial^2 \psi\left(\boldsymbol{\varepsilon}^{\mathrm{e}}\right)}{\partial \boldsymbol{\varepsilon}^{\mathrm{e}} \otimes \partial \boldsymbol{\varepsilon}^{\mathrm{e}}} \tag{5}$$

with $\psi\left(\boldsymbol{\varepsilon}^{\mathrm{e}}\right)$ being the same stored energy function already adopted by [37], [40], [41] – see Appendix for more details.

87 *2.2 Yield function and plastic potential*

88 Yield and plastic potential functions are defined as proposed in [42]:

$$\left.\begin{matrix} f \\ g \end{matrix}\right\} = A_h^{K_{1h}/C_h} B_h^{-K_{2h}/C_h} p' - p'_{sh} = 0 \tag{6}$$

89 with

$$\left.\begin{matrix} K_{1h} \\ K_{2h} \end{matrix}\right\} = \frac{m_h(1-\alpha_h)}{2(1-m_h)} \left\{ 1 \pm \sqrt{1 - \frac{4\alpha_h(1-m_h)}{m_h(1-\alpha_h)^2}} \right\} \tag{7}$$

90

$$\begin{aligned} A_h &= 1 + \frac{1}{K_{1h} M_h(\mathrm{S})} \frac{q}{p'} \\ B_h &= 1 + \frac{1}{K_{2h} M_h(S)} \frac{q}{p'} \\ C_h &= (1-m_h)(K_{1h} - K_{2h}) \end{aligned} \tag{8}$$

91 where the subscript $h = f, g$ is used to indicate either the yield function or the plastic potential. In
92 Equations (6)–(8) m_h and α_h are constitutive parameters (see Table 1). The interested reader is referred
93 to [34], [41], [42], where the physical meaning of relevant model parameters is described.
94 The current stress state is represented through the following three invariants:

$$p' = \frac{1}{3}\mathrm{tr}(\boldsymbol{\sigma}') \qquad q = \sqrt{\frac{3}{2}}\|\mathbf{s}\| \qquad S = \sin(3\theta) = \sqrt{6}\frac{\mathrm{tr}(\mathbf{s}^3)}{\left[\mathrm{tr}(\mathbf{s}^2)\right]^{3/2}} \tag{9}$$

95 where p' is the mean effective stress, q the deviator stress (proportional to the norm of the deviator stress
96 tensor $\mathbf{s}$), and S a trigonometric function of the Lode angle θ (with θ equal to 30° in triaxial compression
97 and -30° in triaxial extension). The variable M_h (S) in Equation (8) is given after [43]:

$$M_h(S) = \frac{2cM_{ch}}{(1+c)-(1-c)S} \qquad c = \frac{M_{eh}}{M_{ch}} \tag{10}$$

98 in which M_c and M_e are the values of $M(S)$ associated with triaxial compression and extension,
99 respectively. The internal variables p'_{sh} in Equation (6) govern the size of the yield locus and plastic
100 potential in the effective stress space. In the following, p'_{sf} is simply denoted as p'_s and termed pre-
101 consolidation stress, while p'_{sg} is a dummy variable that does not affect the stress gradient of g.

2.3 Viscoplastic flow rule

The rate of viscoplastic strains is obtained according to the well-known approach proposed by Perzyna [9], [17]:

$$\dot{\boldsymbol{\varepsilon}}^{\mathrm{vp}} = \gamma \Phi(f) \frac{\partial g}{\partial \boldsymbol{\sigma}'} \tag{11}$$

where f and g keep denoting yield and plastic potential functions (Equation (6)), and Φ is commonly referred to as "viscous nucleus". In the same equation, the so-called "fluidity parameter" γ governs the rate-sensitiveness of the solid skeleton ($\gamma=1/\eta$, with η viscosity) and specifically the rate at which viscoplastic strains occur. Increasing γ values reduce the rate-sensitiveness of the material: when $\gamma \to \infty$ the mechanical response tends to its elasto-plastic (rate-insensitive) limit. At variance with rate-independent plasticity, the magnitude of the viscoplastic strain rate results directly from the scalar "distance" Φ between the current stress point and the yield locus (overstress), with no enforcement of the usual consistency condition. The direction of the instantaneous viscoplastic flow is still governed by the gradient of the plastic potential g.

The selection of the viscous nucleus function is a distinctive feature of elasto-viscoplastic Perzyna models. It must be formulated and calibrated to pursue best agreement with experimental data from standard creep tests, particularly by mobilising in experiments different levels of overstress. It should be noted that the shape of the viscous nucleus function (and associated parameters) is model-specific, i.e. affected by all other (elasto-plastic) features of the model. A more comprehensive discussion on this matter can be found in [1]. Herein, the implications of two different definitions are discussed:

- power-law viscous nucleus, most common in the literature [11]:

$$\Phi(f) = \left\langle \left(\frac{f}{|p'|} \right)^{\alpha} \right\rangle = \left\langle \bar{f}^{\alpha} \right\rangle \tag{12}$$

- exponential viscous nucleus, initially proposed in [1] for loose sands:

$$\Phi(f) = \mathrm{e}^{\alpha \bar{f}} \tag{13}$$

where α is in the above definitions an additional viscous parameter controlling the shape of the viscous nucleus function (Table 1). The Macaulay brackets < > are used in Equation (12) according their usual meaning:

$$\left\langle \bar{f}^{\alpha} \right\rangle = \begin{cases} \bar{f}^{\alpha} & \text{if } \bar{f}^{\alpha} \geq 0 \\ 0 & \text{if } \bar{f}^{\alpha} < 0 \end{cases} \tag{14}$$

to make irreversible viscoplastic strains only occur when the stress state lies outside the elastic domain (i.e. when $f > 0$). Both expressions (12) - (13) fulfil the relevant theoretical requirements discussed by [1], while the use of the dimensionless yield function $\overline{f}$ is appropriate for pressure-sensitive materials [44], [45].

2.4 Hardening rule

Under general hydro-mechanical loading paths, the preconsolidation stress p'_s evolves according to the following hardening rule [34], [35]:

$$\dot{p}'_s = \rho_s p'_s \left(\dot{\varepsilon}_v^{vp} + \xi_s \dot{\varepsilon}_s^{vp} \right) - r_{sw} p'_s \dot{S}_w \tag{15}$$

where ρ_s, ξ_s and r_{sw} are material parameters governing mechanical and hydraulic hardening, respectively (Table 1). In particular, the second term at the right-hand side of Equation (15) models phenomenologically the hydraulic bonding effect characterising the response of unsaturated soils. In Equation (15), $\dot{\varepsilon}_v^{vp}$ and $\dot{\varepsilon}_s^{vp}$ are the rates of volumetric and deviatoric viscoplastic strains respectively:

$$\varepsilon_v = \boldsymbol{\varepsilon} : \mathbf{1} \;\; ; \;\; \varepsilon_s = \sqrt{\frac{2}{3}} \left\| \mathbf{e} \right\| \;\; ; \;\; \dot{\varepsilon}_v = \dot{\boldsymbol{\varepsilon}} : \mathbf{1} \;\; ; \;\; \dot{\varepsilon}_s = \sqrt{\frac{2}{3}} \left\| \dot{\mathbf{e}} \right\| \tag{16}$$

where $\boldsymbol{\varepsilon}$ is the strain tensor, ε_v the volumetric strain, ε_s the deviatoric strain and $\mathbf{e}$ is the deviatoric component of the strain tensor:

$$\mathbf{e} = \boldsymbol{\varepsilon} - \frac{1}{3} \mathrm{tr}(\boldsymbol{\varepsilon}) \mathbf{1} \;\; ; \;\; \dot{\mathbf{e}} = \dot{\boldsymbol{\varepsilon}} - \frac{1}{3} \mathrm{tr}(\dot{\boldsymbol{\varepsilon}}) \mathbf{1} \tag{17}$$

2.5 Influence of relative density

Granular materials respond to mechanical perturbations depending on the current void ratio (pycnotropy) and effective confining pressure (barotropy). This essential feature has been successfully captured in the literature through the notion of “state parameter”, which enables to reproduce the behaviour of loose-to-dense materials with a single set of parameters [46]–[51].

Herein, the simpler approach proposed in [38] has been preferred to exploit the lack of the so-called consistency condition. Accordingly, it is possible to incorporate pycnotropy into the viscoplastic formulation by modulating certain constitutive parameters according to the current relative density (or void ratio). This allows to describe the main consequences of dense-to-loose transitions (and vice versa), such as softening and vanishing dilatancy at medium/large strains [32], [38]. As originally proposed in [38], a linear dependence on the relative density is assumed here for the viscosity η, the representative elastic shear modulus (G_0) and the hardening parameter r_{sw}:

$$p_i = p_{Li} + (p_{Di} - p_{Li}) \cdot D_r \tag{18}$$

in which the value of the generic parameter p_i depends on the current relative density D_r and two bounding values, p_{Li} and p_{Di}, set for the loosest and densest reference conditions – here D_r = 20% and D_r = 100% respectively. Current D_r value is updated at each integration step based on the evolving soil volumetric strain [38]. However, such a linear dependence should not be taken for granted, and indeed the following non-linear relationship has been found to perform better for the constitutive parameters ξ_s and ρ_s (see Section 4.1 and [52]):

$$p_i = p_{Li} + (p_{Di} - p_{Li}) D_r^{5(e_{max} - e_{min})} \tag{19}$$

where in this case p_i represents either ξ_s or ρ_s, while e_{max}/e_{min} are the maximum/minimum void ratios of the sand. In the spirit of the present viscoplastic approach, pycnotropy can be simply reproduced through density-dependent parameters. Nonetheless, specific D_r–dependences need to be identified by comparison to experimental results, and may assume the forms exemplified by Equations (18)-(19).

A synopsis of all constitutive parameters and their meaning is given in Table 1. The model as formulated above is suited for hydro-mechanical processes involving unsaturated conditions and viscous effects. Its performance in presence of strain localisation problems may be fully regularised by coupling viscoplasticity and extension to non-locality ([53]−[55]). This can be easily achieved through a non-local reformulation of the viscoplastic flow-rule Equation (11), as successfully attempted in a few previous works of the authors ([32], [33], [44], [38], [56]−[58]).

The following sections address the calibration and validation of the proposed constitutive model against the response of clean Hostun sand. Although conceived for generally unsaturated sands, the model will be solely tested for either saturated or dry conditions, due to the dearth of test data regarding the rate-sensitiveness of unsaturated sands. The goal is to investigate to what extent a single set of elastic, plastic and viscous parameters can be identified to capture sand response over a wide range of relative density, initial/drainage conditions, loading rate and stress paths.

The model described above has been implemented in the finite element code for multiphase porous media Comes-Geo, developed at the University of Padova ([33], [59]−[66]). All the numerical results have been obtained via explicit forward Euler stress-point integration [67], [68] after preliminary verification of the numerical implementation (see [52]) against the simulation results in Buscarnera and Nova (2009)[1].

[1] It is always possible to compare the performance of a viscoplastic model to the response of its elasto-plastic (rate-insensitive) counterpart by simply setting a sufficiently high fluidity parameter γ in Equation (11).

3 MODEL CALIBRATION FOR LOOSE AND DENSE HOSTUN SAND

All constitutive parameters have been calibrated based on literature triaxial and creep tests on Hostun sand, allowing a separate identification of elasto-plastic and viscous parameters, respectively. Table 2 summarises the main features (drainage, initial confinement and void ratio) of the reference tests from [50], [1], [8], [69]–[70] – the same test labels as in the original publications have been kept in the following.

3.1 Elasto-plastic parameters

The parameters governing the elasto-plastic behaviour have been calibrated by assuming a very high loading rate, i.e. by artificially forcing the response of the viscoplastic model towards its rate-insensitive limit. For this purpose the triaxial test results labelled in Table 2 as *hos027 d4*, *batr02* and *alert9* have been best-matched as exemplified in Figure 1. The final set of calibrated elasto-plastic parameters is reported in Table 3 and Table 4, with the latter providing the loose-to-dense range of D_r-dependent parameters.

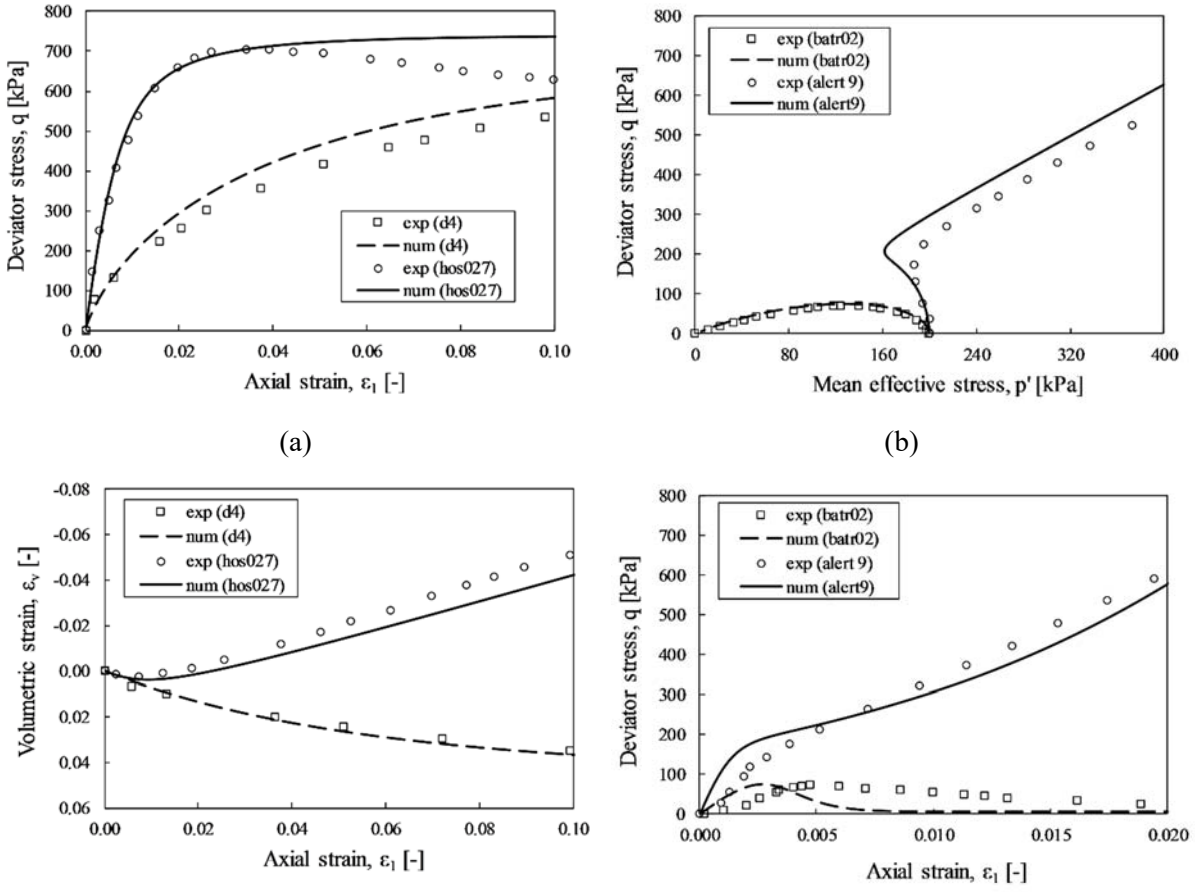

Figure 1: Calibration of elasto-plastic parameters against (a), (c) drained and (b), (d) undrained triaxial test results for loose (*d4, batr02*) and dense (*hos027, alert9*) Hostun sand.

3.2 Viscous parameters

With the same set of elasto-plastic parameters (Tables 3-4), the viscous parameters of Hostun loose and dense sand have been separately identified through the drained creep test results from [1] and [8]. di Prisco and Imposimato [1] performed tests on loose Hostun sand (D_r = 20 %) by holding the radial effective stress constant while increasing the axial component up to attain the target stress obliquity; subsequent axial stress increments have been then applied with a five minutes time lag to explore the creep response. Two sets of viscous parameters have been calibrated for the different viscous nucleus definitions in Equations (12)-(13), namely linear (α=1 in the power-law expression) and exponential. With reference to the last creep step in the original publication (approximately 15 minutes duration), Figure 2 shows the axial strain vs time performance of the model (solid lines) in comparison to the experimental data from [1] (circular markers). It is readily apparent that satisfactory agreement can be achieved in this case regardless of the adopted viscous nucleus, as long as suitable (and nucleus-specific) viscous parameters are set (see Table 5).

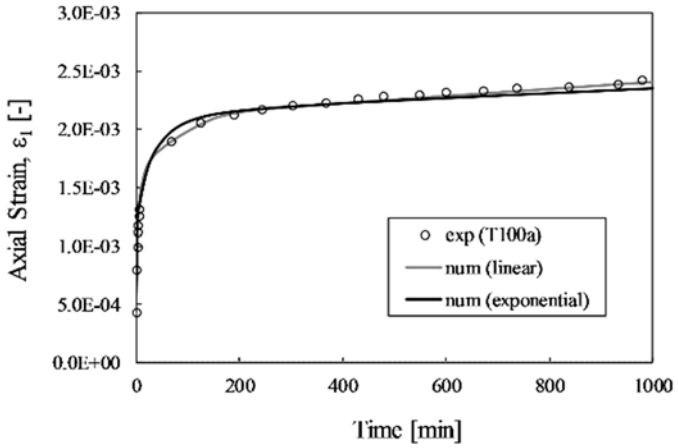

Figure 2: Simulation of loose Hostun sand creep by using linear and exponential viscous nuclei (e_0=0.950, p'_0=100 kPa): axial strain vs time.

The viscous parameters for Hostun dense sand (D_r = 71 %[2]) have been then derived based on the experimental results from [8] and reported in Table 6. It should be noted that the same value of α (i.e. same shape of Φ) has been used for both loose and dense Hostun sand (see Table 5 and Table 6) to reduce the number of free parameters. Such assumption is reasonably confirmed by data/simulations presented herein for Hostun sand, although future confirmation for different materials is needed. The

[2] Given the low viscosity of dense sands, the viscosity identified for D_r = 71 % has been used as p_D in Eq. (18).

laboratory experiments were performed by initially consolidating the sample under an effective mean pressure of 80 kPa, then followed by drained triaxial compression; the triaxial compression load path included three additional stages of creep and cyclic loading, as illustrated in Figure 3.

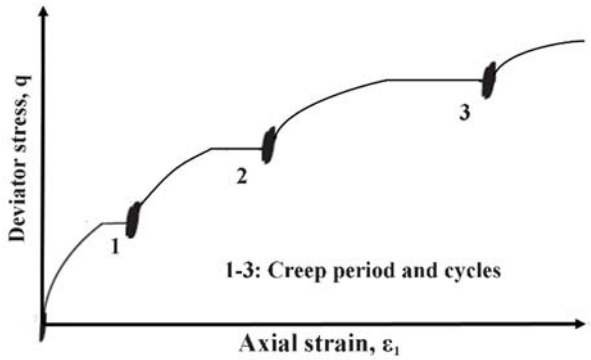

Figure 3: Creep test on dense Hostun sand (after [8]).

Experimental and numerical stress-strain curves are presented in Figure 4a for all four creep stages – no intermediate cyclic loading simulated. For clearer visualisation in Figure 4b, the numerical axial strains developed during creep after each triaxial compression are compared to the experimental results only for the case of exponential viscous nucleus.

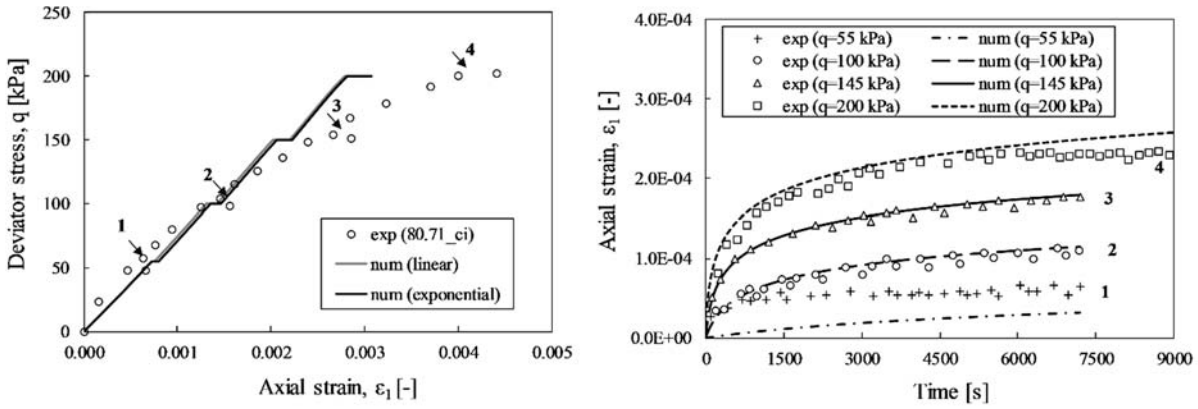

(a) (b)

Figure 4: Simulation of creep behaviour for dense Hostun sand (e_0=0.710, p'_0=80 kPa): (a) global stress-strain response and (b) time evolution of axial strain.

The viscoplastic model reproduces with sufficient accuracy the response to all creep stages, though with some visible deviations from the global stress-strain behaviour (possibly affected by neglecting intermediate cyclic loading in the numerical simulations). Comparing the creep responses of loose and dense Hostun sands points out more significant time effects for the former – in expected agreement with the experimental literature.

4 MODEL VALIDATION

After the above parameter calibration, the full elasto-viscoplastic model is validated against the data set overviewed in Table 2. Such a validation is carried out for Hostun sand at two levels: (i) against triaxial test results already used for the calibration of elasto-plastic parameters (Section 3.1); (ii) against different experimental results – not previously considered – to produce valuable blind predictions. It should be noted that the validation level (i) is still necessary to check whether the parameters derived from creep tests produce appropriate time-sensitiveness when combined with different loading rate and test conditions. The suitability of assuming D_r-dependent constitutive parameters is also highlighted in this section.

All numerical simulations have been performed at imposed displacement rates of 1 mm/min and 2 mm/min for drained and undrained triaxial tests, respectively [72] – unless differently specified.

4.1 Drained triaxial compression tests (TXD)

The model is first validated against the experimental results of TXD tests at varying relative density and effective confinement. The predicted responses arising from the above viscous nucleus definitions are also critically compared, with all relevant material parameters listed in Table 3 to Table 6. A linear D_r-dependence (Equation (18)) is in some instances applied to all variable parameters, so as to point out the better performance the non-linear relationship (19) conclusively applied to the parameters ξ_s and ρ_s. Further insight into the accuracy of the model is provided by comparison to the elasto-plastic predictions obtained through the kinematic-hardening constitutive model of Gajo and Wood [50].

4.1.1 Loose Hostun sand

The outcomes of the two different viscous nuclei (Equations (12)-(13)) are compared in Figure 5 for the TXD response of a loose sample (*d4* in Table 2). The results clearly witness the superior performance of the non-linear/exponential viscous nucleus, which confirms the quite complex dependence of sand viscosity on the overstress level (i.e. on the value of f). It should be noted that the mismatching TXD predictions in Figure 5 come after the same level of accuracy achieved by both viscous nuclei in slow creep tests (Figure 2). This conclusion is also confirmed by the cases of medium dense and dense Hostun sand discussed in the following.

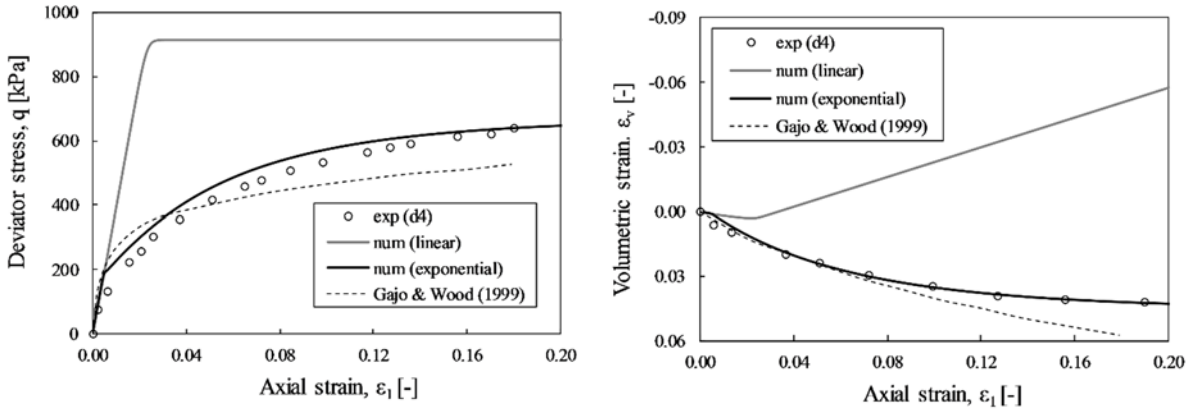

(a) (b)

Figure 5: TXD test on loose Hostun sand (e_0=0.945, p'_0=300 kPa): (a) deviatoric stress-strain response and (b) volumetric behaviour.

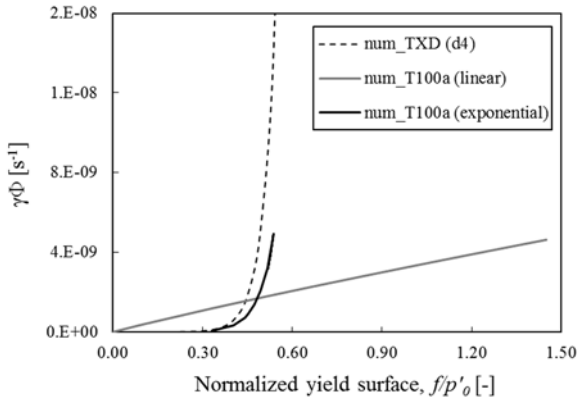

Figure 6: Evolution of the $\gamma\Phi$ product for creep (*T100a*) and TXD (*d4*) tests on loose Hostun sand.

The applicability of the exponential viscous nucleus is underpinned by Figure 6, where the evolution of the $\gamma\Phi$ product (fluidity parameter times viscous nucleus) is plotted against the yield function values for the above TXD (*d4*) and creep (*T100a*) tests. Apparently, the linear viscous nucleus leads to very high values of the yield surface, at variance with the exponential formulation. This stems from the interaction between the functions assumed in this study for the viscous nucleus and the yield locus [42], with the latter being in turn a (very) non-linear function of the (over)stress state. The effect of such interaction stands out under high(er) overstress levels, therefore more clearly under traxial loading than during creep.

4.1.2 Dense Hostun sand

The comparison between experimental and numerical dense sand behaviour is illustrated in Figure 7 (*hos027* in Table 2). As in the loose sand case, the results from the linear viscous nucleus are quite unsatisfactory: the peak stress is significantly underestimated (Figure 7a), while the predicted volumetric

strain trend is less dilative than in reality (Figure 7b). Conversely, the use of exponential nucleus allows to capture correctly both the peak stress and the dilatancy, although the strain softening behaviour can only be reproduced via the non- linear *Dr*-dependence of ξ_s and ρ_s (Equation (19)).

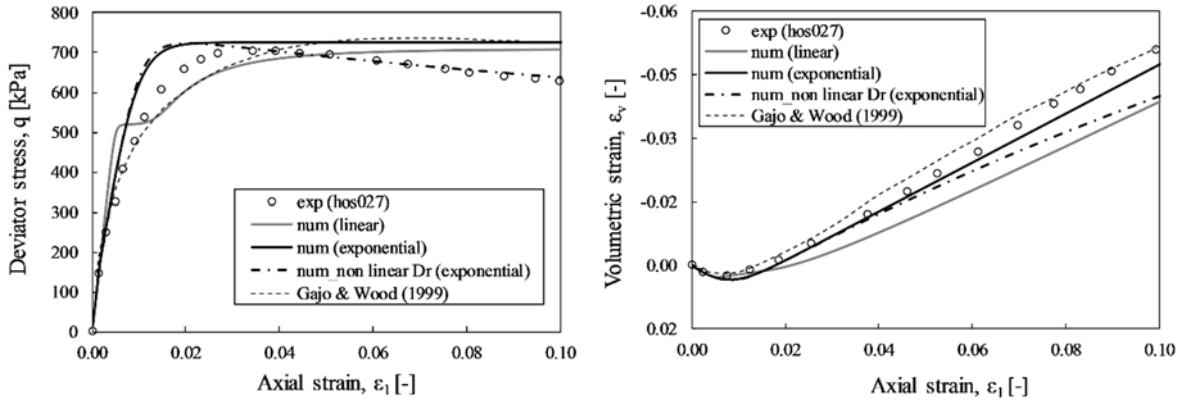

(a) (b)

Figure 7: TXD test on dense Hostun sand (e_0=0.578, p'_0=200 kPa): (a) deviatoric stress-strain response and (b) volumetric behaviour.

4.1.3 Medium dense Hostun sand

The TXD tests on medium-dense Hostun sand are well simulated by the model enhanced with non-linear D_r-dependence – see Figure 8. The peak deviator stress is perfectly matched in Figure 8a, as well as the overall volumetric response in Figure 8b.

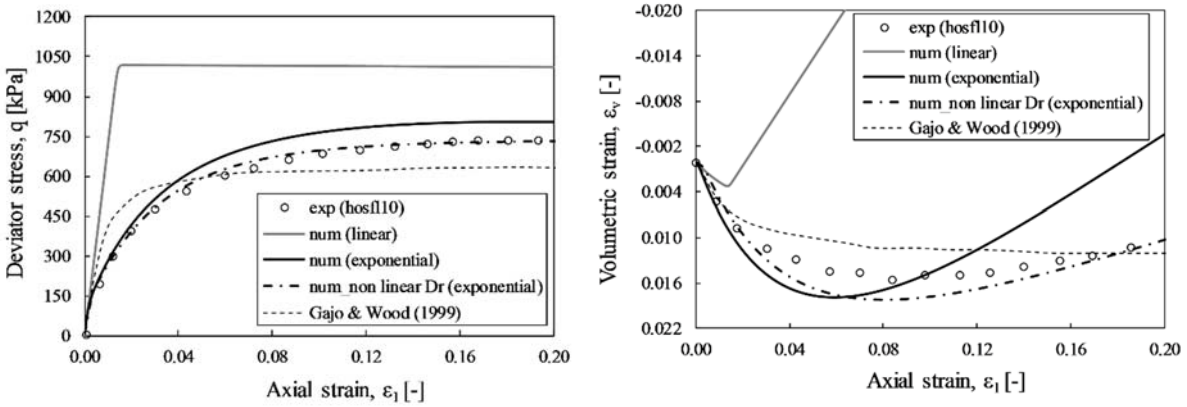

(a) (b)

Figure 8: TXD test on medium-dense Hostun sand (e_0=0.8, p'_0=300 kPa): (a) deviatoric stress-strain response and (b) volumetric behaviour.

4.1.4 Further TXD model predictions

Additional TXD predictions are reported hereafter to further validate the viscoplastic model in its final version with exponential viscous nucleus and non-linear D_r-dependence of the hardening parameters in Equation (19). Experimental vs numerical comparisons are given in Figure 9 for TXD tests on loose

Hostun samples at different confining pressures, namely 100 (*CD-1*), 300 (*CD-2*) and 750 (*CD-3*) kPa – experimental data from [69].

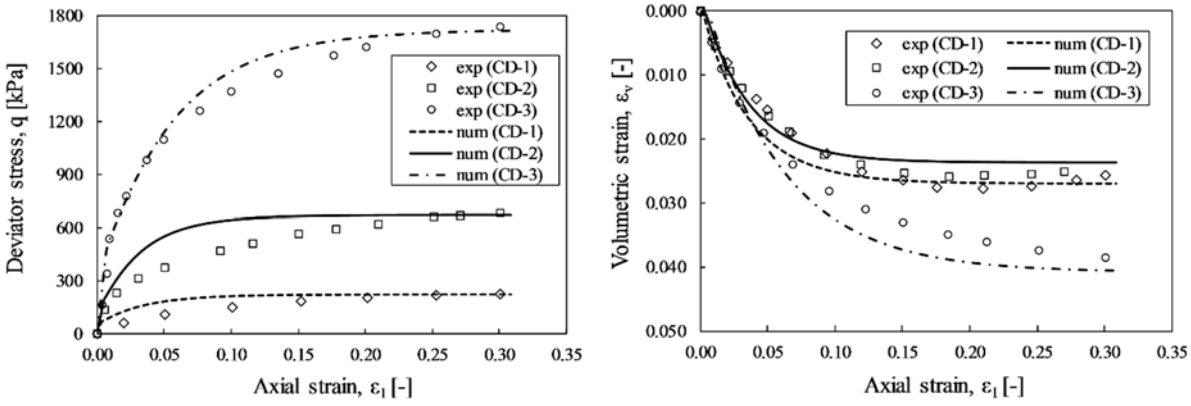

(a) (b)

Figure 9: TXD tests on loose Hostun sand at varying effective confinement (e_0=0.954-1.052, p'_0=100, 300, 750 kPa): (a) deviatoric stress-stress response and (b) volumetric behaviour.

The stress-strain curves and volumetric trends in Figure 9 confirm that model can capture the intrinsic pressure-dependence of sand behaviour at a given relative density (Dr≈10%), with rate-effects spontaneously accommodated by the combination of suitable viscous parameters and realistic TXD loading rate. Relatedly, Figure 10 presents the model predictions obtained for dense and loose Hostun samples initially consolidated under the same isotropic pressure of 300 kPa. For the dense sample, both strain softening behaviour (Figure 10a) and dilation (Figure 10b) are satisfactorily simulated with respect to the experimental results from [50] – test *hos011* in Table 2. Similar conclusions may be extended to the loose sample case – test *hosfl11* (Figure 10c-d).

Figure 11, shows the case of two medium dense Hostun specimens initially consolidated at either low or medium/high effective pressures, 50 kPa (test *hosfl14*) and 600 kPa (test *hflw10*). As expected, the performance of the model is slightly worse – though not dramatically – for intermediate void ratios, for which more accurate modelling of barotropy/pycnotropy is likely needed.

The last TXD simulations in Figure 12 allow to further inspect the rate-sensitiveness of the monotonic triaxial response. For this purpose, the experimental results on air-dried loose Hostun sand from [8] have been considered, including isotropic consolidation up to 400 kPa followed by axial straining at two different rates – one 10 times larger than the other. Even though Perzyna-type models are necessarily sensitive to the loading rate until the inviscid limit, such sensitivity must be quantitatively compared to experimental evidence. In agreement with previous/related sources (see e.g. [3], [15]), the experimental results in Figure 12 confirm negligible rate-dependence of Hostun sand at the considered constant strain rates – note the almost coincident stress–strain curves. Elasto-viscoplastic simulations with unaltered

constitutive parameters display in this case underpredicted sand stiffness, but confirm the observed low rate-sensitiveness of the material. The merit for the latter outcome comes mostly from the adopted viscous nucleus formulation, suitable to capture (drained) rate-sensitiveness over a wide overstress range.

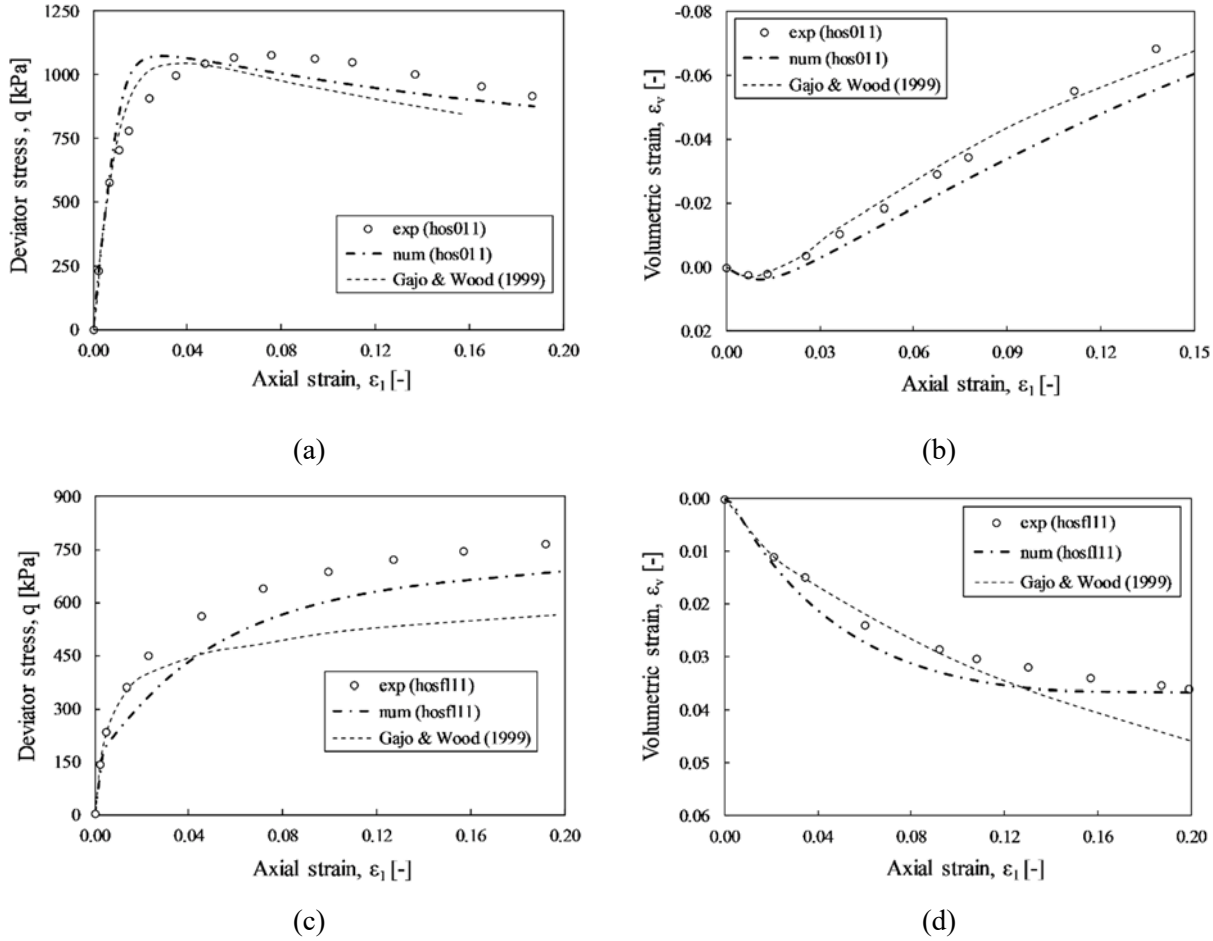

Figure 10: TXD tests on dense (e_0=0.574) and loose (e_0=0.897) Hostun sand at the same effective confinement (p'_0=300 kPa): (a)-(c) deviatoric stress-stress response and (b)-(d) volumetric behaviour.

Overall, the results in this section show good ability of the model to reproduce TXD tests at varying initial void ratio, effective confinement and loading rate, with viscous parameters independently identified from creep experiments. This achievement is not dramatically affected by the unavoidable heterogeneity of materials, facilities and operators in the reference experimental studies.

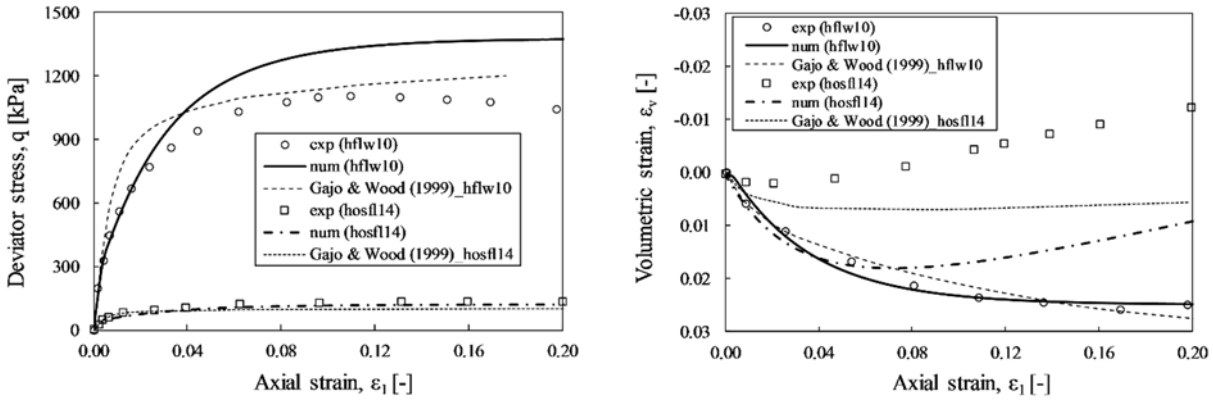

(a) (b)

Figure 11: TXD tests on medium dense (e_0 = 0.822-0.838) Hostun sand and different effective confinement (p'_0=50, 600 kPa): (a) deviatoric stress-stress response and (b) volumetric behaviour.

309

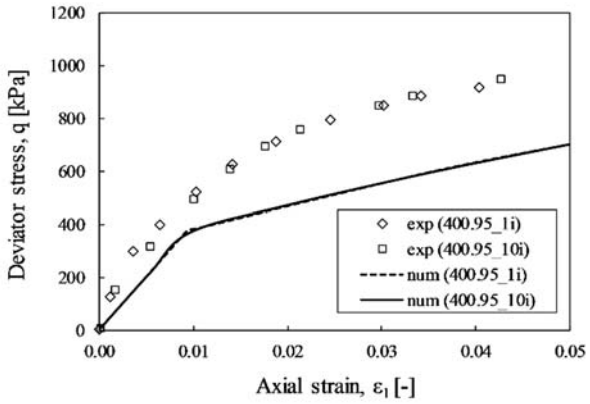

Figure 12: TXD on air-dried loose Hostun sand (e_0 = 0.95) performed, respectively, at a strain rate of $\dot{\varepsilon}_0$ = 0.06 %/min, test 400.95 1i and $\dot{\varepsilon}_0$ = 0.6 %/min, test 400.95 10i (data from [8][3]) .

310 *4.2 Undrained triaxial compression tests (TXU)*

311 In this subsection the undrained triaxial performance of the proposed model is explored with respect
312 to the TXU tests in Table 2. It is noted that transiting to undrained conditions jeopardises the suitability
313 of the viscous parameters in Tables 5-6, which leads to envisage $\Phi(f)$ function probably more complex
314 than the assumed exponential form [56]. The different stress paths characterising TXD and TXU tests
315 mobilise different ranges of the Φ-f relationship, whose non-linearity should be captured for accurate
316 simulations over a wide spectrum of loading conditions. Relatedly, simplistic viscous nucleus

[3] Intermediate relaxation branches in the original data have been removed from the plot, as overlooked in the numerical simulations for the sake of simplicity.

317 formulation conceived, for instance, for numerical regularisation purposes, may yield misleading results
318 when applied to very diverse loading/drainage conditions.

319 The parameters of the exponential viscous nucleus have been thus recalibrated based on the TXU
320 results in Figures 13-14, for loose and dense Hostun sand respectively – tests *batr02* and *alert9* from
321 [50]. The same figures indicate that the new viscous parameters in Table 7 along with the above elasto-
322 plastic parameters (Tables 3-4) result in reasonable simulations of undrained stress paths and deviatoric
323 stress-stress responses for both loose and dense samples. It is also worth observing that the D_r-
324 dependence of constitutive parameters is here only relevant to setting proper initial conditions, as the
325 void ratio does not vary during TXU loading.

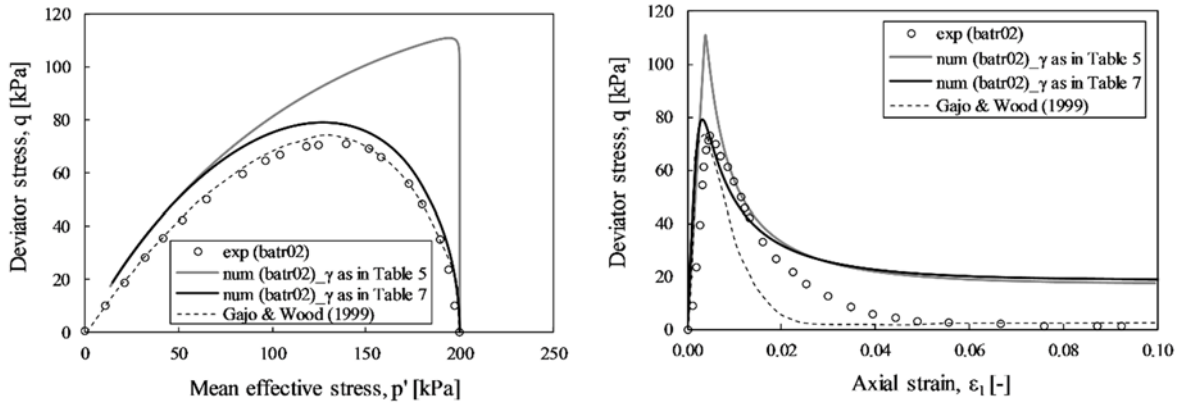

(a) (b)

Figure 13: Re-calibration of the viscous parameters against TXU test on loose Hostun sand (e_0=0.940, p'_0=200 kPa): (a) stress path and (b) deviatoric stress-stain response.

326

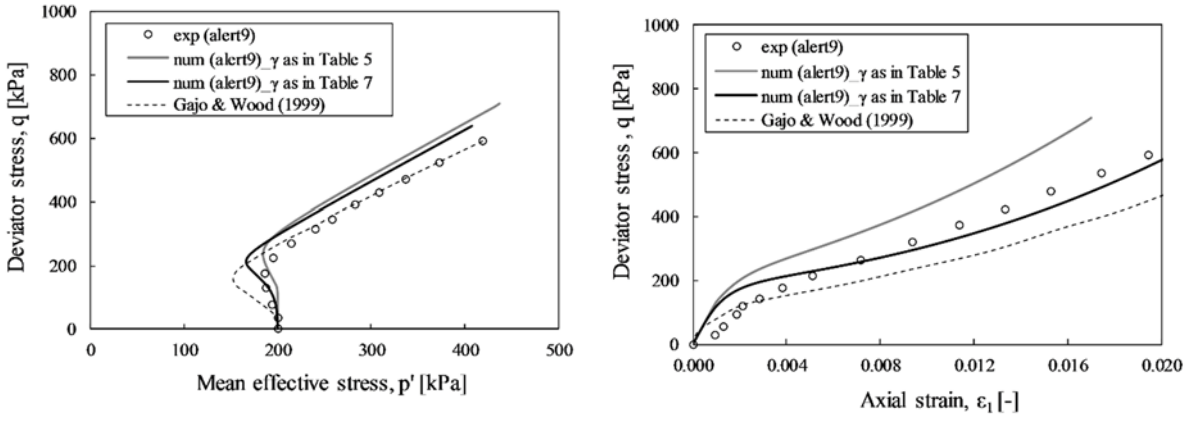

(a) (b)

Figure 14: Re-calibration of the viscous parameters against TXU test on dense Hostun sand (e_0=0.666, p'_0=200 kPa): (a) stress path and (b) deviatoric stress-stain response.

327

After the identification of "undrained" viscous parameters, TXU tests on loose and medium-dense Hostun specimens have been considered for re-validation. The results in Figure 15 concern the tests from [69] on loose sand at initial confinement equal to 750kPa (*ICU-1*), 300kPa (*ICU-2*) and 100kPa (*ICU-3*). Encouraging numerical predictions have been found again in all relevant respects, and particularly in terms of undrained stress path and pore pressure build-up. Similar satisfactory results can be seen in Figure 16 for the medium dense sand tested by [50] – test *batr06*.

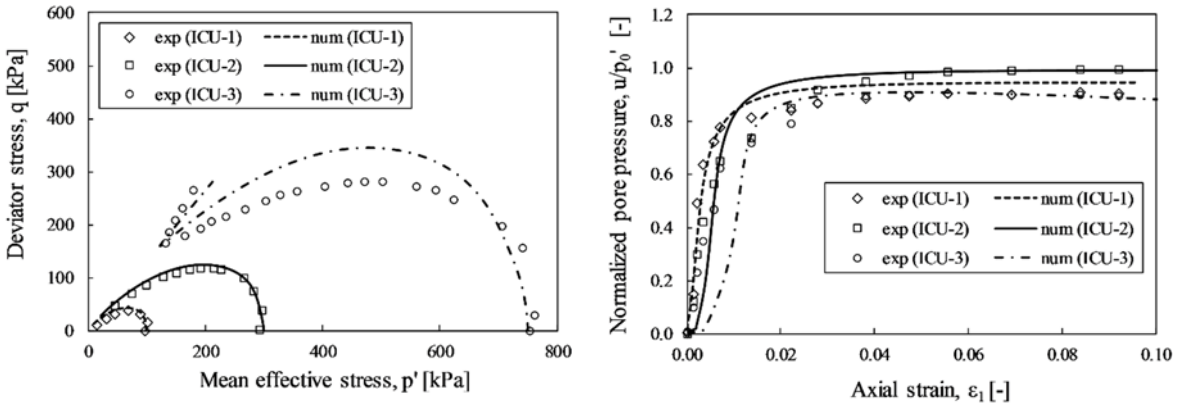

(a) (b)

Figure 15: TXU tests on loose Hostun sand at varying effective confinement (e_0=1.060-1.083, p'_0=100, 300, 750 kPa): (a) stress path and (b) normalized pore pressure versus axial strain.

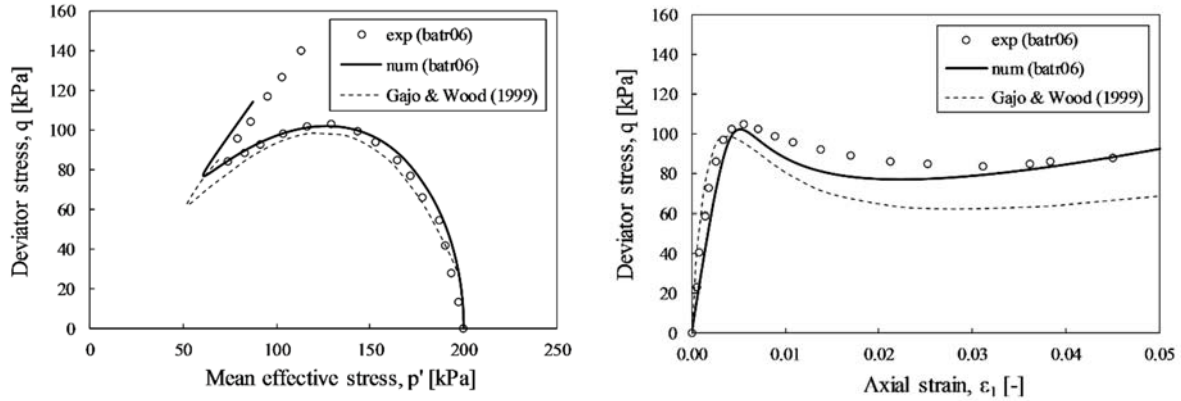

(a) (b)

Figure 16: TXU on medium-dense (e_0=0.830, p'_0=200 kPa) Hostun sand: (a) stress path and (b) deviatoric stress-stain response.

4.3 Undrained plane-strain/biaxial compression test

Further validation has been successfully sought against the biaxial undrained test results documented in [70] – test *SHFND05*, p'_0=800 kPa, axial displacement rate equal to 1.2 mm/min. Similarly to drained conditions, the model endowed with its "undrained" viscous nucleus is capable to blindly predict other experimental data not used for calibration. Specifically, Figure 17 illustrates the excellent agreement achieved in terms of stress path, stress-strain response and pore pressure build up.

4.4 Undrained creep tests

The results of (rare) undrained creep tests on Hostun loose sand are used as a final benchmark – data from [71]. The original experimental tests were conducted with undrained creep following a preliminary TXD stage up to target stress obliquity. Such a loading programme (test *20DP13*) has been simulated with the same parameters mentioned in Sections 4.2-4.3. During the TXD phase small load increments were applied: between two subsequent load increments a time period of 5 minutes elapsed; when the desired stress level was reached (q = 61 kPa, p' = 120 kPa) a further load increment of 2 kPa was applied. The predictions in Figure 18 obtained for the creep stage show reasonable agreement in terms of axial strain and pore pressure. The premature onset of creep instability (inflection point in the pore pressure curve) is most likely due to the specific yield function shape and the (simplistic) assumption of isotropic hardening ([25], [75]), rather than to viscous modelling.

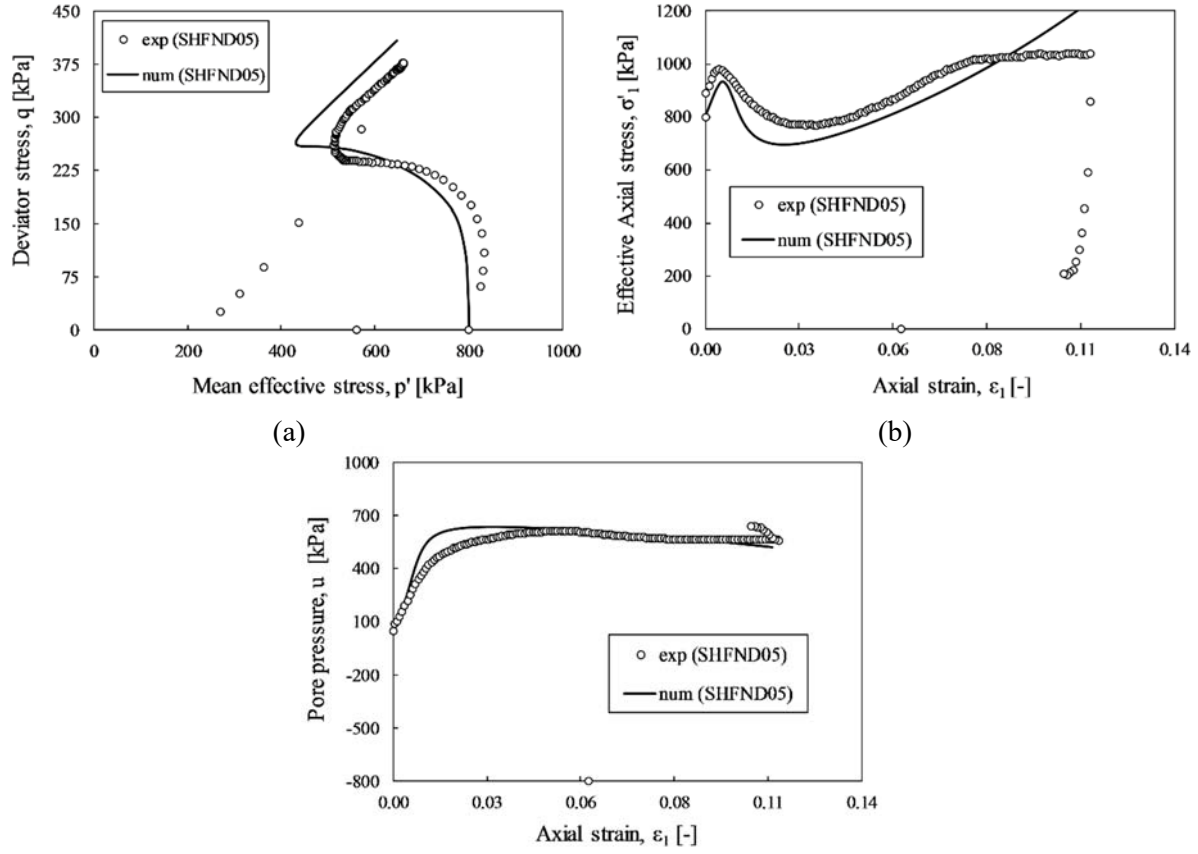

(a) (b)

(c)

Figure 17: Biaxial test on loose Hostun sand (e_0=0.945, p'_0=800 kPa): (a) stress path, (b) deviatoric stress-stain response, (c) pore pressure build-up.

354

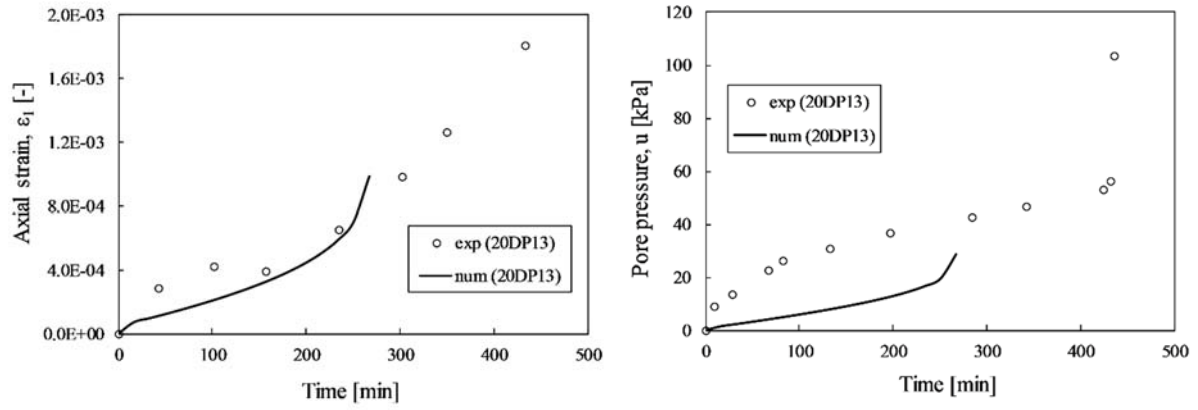

(a) (b)

Figure 18: Undrained creep test on loose Hostun sand (e_0=0.900, p'_0=100 kPa): time evolution of (a) axial strain and (b) pore pressure.

355

5 CONCLUSIONS

An existing elasto-plastic model for sandy soils was reformulated as a Perzyna viscoplastic relationship to capture the rate-sensitive, pycnotropic and barotropic behaviour of sands under different loading/initial/boundary and drainage conditions. In particular, the suitability of two alternative viscous nucleus definitions, namely linear and exponential, was verified with respect to both creep and triaxial test data on Hostun sand from the literature. Importantly, the parameters governing the time-dependence of the material were separately calibrated against creep tests and then found suitable to reproduce the different loading paths/rates induced during standard triaxial tests. While the need for quite complex viscous nucleus functions was confirmed, it was also shown how challenging still is to unify the simulation of both drained and undrained responses under a single analytical formulation with a unique set of material parameters. Unlike most literature on the subject, this work highlights that simplistic assumptions about rate-sensitiveness may abruptly reduce the predictive potential of elasto-viscoplastic models.

From a modelling perspective, it should be noted that quantitative conclusions on the predictive range are very specific of both the viscous nucleus and yield functions adopted. The non-linearity needed of the viscous nucleus Φ for good match with real data relates necessarily to how non-linear the f function is. When inherited from existing elasto-plastic formulations for granular soils, capped yield loci and plastic potentials are most often very non-linear, as necessary to capture the response under diverse loading programmes (including e.g. radial stress paths). This fact not only makes extension to viscoplasticity less straightforward, but also poses conceptual questions about the effects of convexity losses experienced by these functions in the overstress regime (i.e. outside the f=0/g=0 loci). Expected consequences might concern the predicted stability of the constitutive response [23], a subject so far never explored from this standpoint. When documented, convexity-related issues might be remedied by resorting to recent convexification techniques ([73], [74]).

The discussion offered in this work also aimed to discourage simplistic use of viscoplasticity as a mere numerical expedient against mesh-dependence in strain-localisation problems. Conversely, the viscoplastic framework was reappraised as a physically sound approach to sand modelling, easy to extend to non-locality whenever also characteristic length effects are relevant.

ACKNOWLEDGMENTS

The authors wish to thank the 7th Framework Programme of the European Union (ITN MuMoLaDe project 289911) and the University of Padova for financially supporting this work. The valuable input of Giuseppe Buscarnera and Constance Mihalache (Northwestern University) and Jacques Desrues (Université de Grenoble-Alpes) is also gratefully acknowledged.

APPENDIX

Stored energy function and hyperelastic behaviour

The strain energy function $\psi\left(\boldsymbol{\varepsilon}^{\mathrm{e}}\right)$ in Equation (5) is given by the following two-invariant expression:

$$\psi\left(\boldsymbol{\varepsilon}^{\mathrm{e}}\right)=\overline{\psi}\left(\varepsilon_{\mathrm{v}}^{\mathrm{e}},\varepsilon_{\mathrm{s}}^{\mathrm{e}}\right)=\tilde{\psi}\left(\varepsilon_{\mathrm{v}}^{\mathrm{e}}\right)+\frac{3}{2}\left[G_{0}+\frac{\mathsf{a}}{\hat{k}}\tilde{\psi}\left(\varepsilon_{\mathrm{v}}^{\mathrm{e}}\right)\right]\left(\varepsilon_{\mathrm{s}}^{\mathrm{e}}\right)^{2} \tag{20}$$

where:

$$\tilde{\psi}\left(\varepsilon_{\mathrm{v}}^{\mathrm{e}}\right)=\begin{cases}\hat{k}p_{r}\exp\left(\dfrac{\varepsilon_{\mathrm{v}}^{\mathrm{e}}}{\hat{k}}-1\right), & \varepsilon_{\mathrm{v}}^{\mathrm{e}}\geq\hat{k}\ \left(\text{or } p'\geq p_{r}\right)\\ p_{r}\varepsilon_{\mathrm{v}}^{\mathrm{e}}+\dfrac{p_{r}\left(\varepsilon_{\mathrm{v}}^{\mathrm{e}}-\hat{k}\right)^{2}}{2\hat{k}}, & \varepsilon_{\mathrm{v}}^{\mathrm{e}}<\hat{k}\ \left(\text{or } p'<p_{r}\right)\end{cases} \tag{21}$$

This model produces pressure-dependent bulk and shear elastic moduli. $G_{0},\hat{k},\mathsf{a}$ are constitutive parameters, p_r is a reference mean effective stress, while ε_{v}^{e}, ε_{s}^{e} are the elastic volumetric strain and the second invariant of the elastic strain deviator, respectively. When $p'<p_r$ the hyperelastic law predicts a linear elastic behaviour, whereas a fully non-linear pressure dependent behaviour is obtained for $p'\geq p_r$. By taking the first and the second derivative of Equation (20) with respect to $\boldsymbol{\varepsilon}^{\mathrm{e}}$, the following expressions for the stress and the elastic stiffness tensor are obtained:

$$\boldsymbol{\sigma}'=\frac{\partial\psi\left(\boldsymbol{\varepsilon}^{\mathrm{e}}\right)}{\partial\boldsymbol{\varepsilon}^{\mathrm{e}}}=\left[1+\frac{3\mathsf{a}}{2\hat{k}}\left(\varepsilon_{s}^{e}\right)^{2}\right]\theta_{\varepsilon}\mathbf{1}+2\left(G_{0}+\frac{\mathsf{a}}{\hat{k}}\tilde{\psi}\right)\mathbf{e}^{\mathrm{e}} \tag{22}$$

and:

$$\mathbf{D}^{\mathrm{e}}=\left[1+\frac{3\mathsf{a}}{2\hat{k}}\left(\varepsilon_{s}^{e}\right)^{2}\right]K_{\varepsilon}\mathbf{1}\otimes\mathbf{1}+2\left(G_{0}+\frac{\mathsf{a}}{\hat{k}}\tilde{\psi}\right)\left[\mathbf{I}-\frac{1}{3}\mathbf{1}\otimes\mathbf{1}\right]+2\left(\frac{\mathsf{a}}{\hat{k}}\right)\theta_{\varepsilon}\left(\mathbf{1}\otimes\mathbf{e}^{\mathrm{e}}+\mathbf{e}^{\mathrm{e}}\otimes\mathbf{1}\right) \tag{23}$$

where, $\mathbf{e}^{\mathrm{e}}=\boldsymbol{\varepsilon}^{\mathrm{e}}-\frac{1}{3}\mathrm{tr}(\boldsymbol{\varepsilon}^{\mathrm{e}})\mathbf{1}$ is the deviatoric elastic strain and:

$$\theta_{\varepsilon}=\frac{\partial\tilde{\psi}\left(\varepsilon_{\mathrm{v}}^{\mathrm{e}}\right)}{\partial\varepsilon^{\mathrm{e}}}=\begin{cases}p_{r}\exp\left(\dfrac{\varepsilon_{\mathrm{v}}^{\mathrm{e}}}{\hat{k}}-1\right), & \varepsilon_{\mathrm{v}}^{\mathrm{e}}\geq\hat{k}\ \left(\text{or } p'\geq p_{r}\right)\\ p_{r}\dfrac{\varepsilon_{\mathrm{v}}^{\mathrm{e}}}{\hat{k}}, & \varepsilon_{\mathrm{v}}^{\mathrm{e}}<\hat{k}\ \left(\text{or } p'<p_{r}\right)\end{cases} \tag{24}$$

$$K_{\varepsilon} = \frac{\partial \theta_{\varepsilon}}{\partial \varepsilon^{\mathrm{e}}} = \begin{cases} \dfrac{p_r}{\hat{k}} \exp\left(\dfrac{\varepsilon_{\mathrm{v}}^{\mathrm{e}}}{\hat{k}} - 1 \right), & \varepsilon_{\mathrm{v}}^{\mathrm{e}} \geq \hat{k} \left(\text{or } p' \geq p_r \right) \\ \dfrac{p_r}{\hat{k}}, & \varepsilon_{\mathrm{v}}^{\mathrm{e}} < \hat{k} \left(\text{or } p' < p_r \right) \end{cases} \tag{25}$$

403

404 **REFERENCES**

405 [1] di Prisco C, Imposimato S. Time dependent mechanical behaviour of loose sands. *Mechanics of*
406 *Cohesive-Frictional Materials* 1996; **1**: 45–73.

407 [2] Lade PV, Yamamuro JA, Bopp PA. Influence of time effects on instability of granular materials,
408 *Computers and Geotechnics* 1997; **20**(3-4):179–193.

409 [3] Tatsuoka F, Jardine RJ, Lo Presti D, Di Benedetto H, Kodaka, T. Characterising of the Pre-Failure
410 Deformation Properties of Geomaterials. *Proceedings of the 14th International Conference on Soil*
411 *Mechanics and Foundation Engineering*, Hamburg, Germany, 2129–2164, 1997.

412 [4] Di Benedetto H, Tatsuoka F. Small strain behavior of geomaterials: modelling of strain rate effects.
413 *Soils and Foundations* 1997; **37**(2): 127–138.

414 [5] Di Benedetto H, Ibraim E, Cazacliu B. Time dependent behaviour of sand. *Proceedings of the 2nd*
415 *International Symposium on Pre-failure Deformation Characteristics of Geomaterials*, Torino,
416 Italy, Jamiolkowski M et al. (eds), 459–466, 1999.

417 [6] Di Benedetto H, Tatsuoka F, Lo Presti D, Sauzéat C, Geoffroy H. Time effects on the behaviour of
418 geomaterials, *Deformation Characteristics of Geomaterials: Recent Investigations and Prospects*,
419 Di Benedetto et al. (eds). Taylor & Francis Group, London, 59–123, 2005.

420 [7] Augustesen A, Liingaard M, Lade PV. Evaluation of Time-Dependent Behavior of Soils.
421 *International Journal of Geomechanics* 2004; **4**(3):137–156.

422 [8] Pham Van Bang D, Di Benedetto H, Duttine A, Ezaoui A. Viscous behaviour of dry sand.
423 *International Journal for Numerical and Analytical Methods in Geomechanics* 2007; **31**: 1631–
424 1658.

425 [9] Perzyna P. The constitutive equations for rate sensitive plastic materials. *Quarterly of Aapplied*
426 *Mathematics* 1963; 20(**4**): 321–332.

427 [10] Duvaut G, Lion JL. *Les inequations en mechanique et en physique*. Dunod:Paris,1972.

428 [11] Wang WM, Sluys LJ, De Borst R. Viscoplasticity for instabilities due to strain softening and
429 strain-rate softening. *International Journal for Numerical Methods in Engineering* 1997; **40** (20):
430 3839–3864.

431 [12] Runesson K, Ristinmaa M, Mähler L. A comparison of viscoplasticity formats and algorithms.
432 Mech. *Cohesive frictional Mater* 1999; **4**(1): 75–98.

433 [13] Carosio A, Willam K, Etse G. On the consistency of viscoplastic formulations. *International*
434 *Journal of Solids and Structures* 2000; **37**(48–50): 7349–7369.

[14] Heeres O, Suiker A, de Borst R. A comparison between the Perzyna viscoplastic model and the Consistency viscoplastic model. *European Journal of Mechanics. A/Solids* 2002; **21**: 1–12.

[15] Di Benedetto H, Tatsuoka F, Ishihara M. Time-dependent shear deformation characteristics of sand and their constitutive modelling. *Soils and Foundations* 2002; **42**(2): 1–22.

[16] Tatsuoka F, Uchimura T, Hayano K, Koseki J, Di Benedetto H, Siddiquee MS. A. Time-dependent deformation characteristics of stiff geomaterials in engineering practice. In M. Jamiolkowski, R. Lancellotta, & D. Lo Presti (Eds.), *Pre-Failure Deformation Characteristics of Geomaterials*, 1161–1250, 1999.

[17] Perzyna P. Fundamental problems in viscoplasticity. *Advances in Applied Mechanics 1966*; **9**: 243–377.

[18] Borja RI. *Modeling the monotonic and cyclic viscoplastic soil behavior. Proceedings of the second International Conference on recent advances in geotechnical earthquake engineering and soil dynamics* (ed. S. Prakash), vo1 1.14: 37–40. Rolla, MO, USA: Missouri University of Science and Technology, 1991.

[19] di Prisco C, Imposimato S, Vardoulakis I. Mechanical modelling of drained creep triaxial tests on loose sand. *Géotechnique* 2000; **50**(1): 73–82.

[20] di Prisco C, Imposimato, S. Static liquefaction of a saturated loose sand stratum, *International Journal of Solids and Structures* 2002; **39**: 3523–3541.

[21] Yin ZY, Chang CS, Karstunen M, Hicher PY. An anisotropic elastic–viscoplastic model for soft clays. *International Journal of Solids and Structures* 2010; **5**: 665–677.

[22] Oka F, Adachi T, Yashima A. Instability of an elastoviscoplastic constitutive model for clay and strain localization. *Mechanics of Materials* 1994; **18**: 119–129.

[23] Pisanò F, di Prisco C. A stability criterion for elasto-viscoplastic constitutive relationships. *International Journal for Numerical and Analytical Methods in Geomechanics* 2015; **40**(1): 141–156.

[24] Marinelli F, Buscarnera G. Instability criteria for quasi-saturated viscous soils. *International Journal for Numerical and Analytical Methods in Geomechanics* 2017; DOI: 10.1002/nag.2746.

[25] Marinelli F, Pisanò F, di Prisco C, Buscarnera G. Model-based interpretation of undrained creep instability in loose sands. *Géotechnique* 2017; 1–14.

[26] Needleman A. Material rate dependence and mesh sensitivity on localization problems. *Computer Methods in Applied Mechanics and Engineering* 1988; **67**: 69–86.

[27] Loret B, Prevost JH. Dynamic strain localization in fluid-saturated porous media. *Journal of Engineering Mechanics* 1991; **117**(4):907–922.

[28] Sluys LJ. Wave propagation, localisation and dispersion in softening solids. *Ph.D. Thesis*, Delft University of Technology, 1992.

[29] Schrefler B A, Zhang HW, Sanavia L. Fluid-structure interaction in the localisation of Saturated porous media, *Zeitschrift für Angewandte Mathematik und Mechanik (Journal of Applied Mathematics and Mechanics, Z. Angew. Math. Mech.)* 1999; **79**(7): 481–484.

[30] Ehlers W, Graf T, Ammann M. Deformation and localization analysis of partially saturated soil.

Computer Methods in Applied Mechanics and Engineering 2004; **193**: 2885–2910.

[31] Rice JR. *The localisation of plastic deformation. Proceedings of the 14th IUTAM Congress, Koiter W.T. (ed.)*, Delft (North Holland, Amsterdam), 207–220, 1976.

[32] di Prisco C, Imposimato S. Nonlocal numerical analyses of strain localization in dense sand. *Mathematical and Computer Modelling* 2003; **37**: 497–506.

[33] Lazari M, Sanavia L, Schrefler BA. Local and non-local elasto-viscoplasticity in strain localization analysis of multiphase geomaterials. *International Journal for Numerical and Analytical Methods in Geomechanics* 2015; **39**:1570–1592.

[34] Buscarnera G, Nova R. An elastoplastic strain hardening model for soil allowing for hydraulic bonding–debonding effects. *International Journal for Numerical and Analytical Methods in Geomechanics* 2009; **33**(8): 1055–1086.

[35] Jommi C. *Remarks on the constitutive modelling of unsaturated soils. Experimental Evidence and Theoretical Approaches in Unsaturated Soils, In Proceedings of an International Workshop*, Trento, 139–153, 2000.

[36] Jommi C, di Prisco C. A simple theoretical approach for modelling the mechanical behaviour of unsaturated soils (in Italian). *In Proceedings of the Conference "Il ruolo dei fluidi nei problemi di Ingegneria geotecnica"*, **1**: 167–188, 1994.

[37] Nova R, Castellanza R, Tamagnini C. A constitutive model for bonded geomaterials subject to mechanical and/or chemical degradation. *International Journal for Numerical and Analytical Methods in Geomechanics* 2003; **27**: 705–732.

[38] di Prisco C, Imposimato S, Aifantis EC. A visco-plastic constitutive model for granular soils modified according to non-local and gradient approaches. *International Journal for Numerical and Analytical Methods in Geomechanics* 2002; **26**: 121–138.

[39] Schrefler BA. The finite element method in soil consolidation (with applications to surface subsidence), *PhD. Thesis*, University College of Swansea, 1984.

[40] Borja RI, Tamagnini C, Amorosi A. Coupling plasticity and energy-conserving elasticity models for clay. *Journal of Geotechnical and Geoenvironmental Engineering* 1997; **123**(10): 948–957.

[41] Tamagnini C, Castellanza R, Nova R. A generalized backward Euler algorithm for the numerical integration of an isotropic hardening elastoplastic model for mechanical and chemical degradation of bonded geomaterials. *International Journal for Numerical Methods in Engineering* 2002; **26**: 963–1001.

[42] Lagioia R, Puzrin A, Potts D. A new versatile expression for yield e plastic potential surfaces. C*omputers and Geothecnics* 1996; **19**(3): 171–191.

[43] Gudehus G. Elastoplastische stoffgleichungen für trochkenen sand. *Infenieyr-Archiv* 1973; **42:** 151–169.

[44] Pisanò F. Seismic Performance of Infinite Earth Slopes: Numerical Modelling, Constitutive Issues and Theoretical Considerations, *Ph.D. Thesis*, Politecnico di Milano, Italy, 2011.

[45] di Prisco C, Pastor M, Pisanò F. Shear wave propagation along infinite slopes: A theoretically based numerical study. *International Journal for Numerical and Analytical Methods in Geomechanics* 2012; **36**(5): 619-642.

514 [46] Uriel S. Intrinsic dynamic of the quasi-static mechanics of granular soils. *In Numerical Methods*
515 *in Soil and Rock Mechanics*, Borm G, Meissher H (eds). Institut fu Bondenmechanik und
516 Felsmechanik der Universitat Karlsruhe: Karlsruhe: 61–70, 1975.

517 [47] Been K, Jefferies MG. A state parameter for sands. *Géotechnique* 1985; **35**(2): 99–112.

518 [48] Wood DM, Belkheir K. Strain softening and state parameter for sand modelling. *Géotechnique*
519 1994; **44**(2): 335–339.

520 [49] Manzari M, Dafalias Y. A critical state two-surface plasticity model for sands. *Géotechnique*
521 1997; **47**(2): 255–272.

522 [50] Gajo A, Wood DM. Seven-Trent sand: a kinematic-hardening constitutive model: the q-p
523 formulation. *Géotechnique* 1999; **49** (5): 595–614.

524 [51] Manzanal D, Fernández-Merodo JA, Pastor M. Generalized plasticity state parameter-based
525 modelling of saturated and unsaturated soils. Part I: saturated state. *International Journal for*
526 *Numerical and Analytical Methods in Geomechanics* 2011; **35**: 1347–1362.

527 [52] Lazari M. Finite element regularization for post localized bifurcation in variably saturated media,
528 *Ph.D. Thesis*, University of Padova, Italy, 2016.

529 [53] Jirasék M. Objective modeling of strain localization. *Revue française de génie civil* 2002; **6**: 119–
530 1132.

531 [54] Jirásek M, Rolshoven S. Comparison of integral-type nonlocal plasticity models for strain-
532 softening materials. *International Journal of Engineering Science* 2003; **41**: 1553–1602.

533 [55] Lu X, Bardet JP, Huang M. Spectral analysis of nonlocal regularization in two-dimensional finite
534 element models. *International Journal for Numerical and Analytical Methods in Geomechanics*
535 2012; **36**: 219–235.

536 [56] di Prisco C, Stupazzini M, Zambelli C. Nonlinear SEM numerical analyses of dry dense sand
537 specimens under rapid and dynamic loading. *International Journal for Numerical and Analytical*
538 *Methods in Geomechanics* 2007; **31**(6): 757–788.

539 [57] Murianni A, Di Prisco C, Federico A. Numerical stability of non-local viscoplastic FEM analyses
540 for the study of localisation processes. *Geomechanics and Geoengineering* 2013; **8**(4): 215–228.

541 [58] Lazari M, Sanavia L, Schrefler BA. Finite element modelling of shear bands in porous media by
542 means of non-local viscoplasticity. *COMPLAS XIII: proceedings of the XIII International*
543 *Conference on Computational Plasticity: fundamentals and applications*, Barcelona: CIMNE,
544 2015, 140–150.

545 [59] Lewis RW, Schrefler BA. *The Finite Element Method in the Static and Dynamic Deformation*
546 *and Consolidation of Porous Media*. John Wiley & Sons, Chichester, 1998.

547 [60] Gawin D, Schrefler BA. Thermo-hydro-mechanical analysis of partially saturated porous
548 materials. *Engineering Computations* 1996; **13**(7): 113–143.

549 [61] Sanavia L, Pesavento F, Schrefler BA. Finite element analysis of non-isothermal multiphase
550 geomaterials with application to strain localization simulation. *Computational Mechanics* 2006;
551 **37**: 331–348.

552 [62] Sanavia L. Numerical Modelling of a Slope Stability Test by Means of Porous Media Mechanics.

553 *Engineering Computations* 2009; **26**(3), 245–266.

554 [63] Gawin D, Sanavia L. A unified approach to numerical modelling of fully and partially saturated
555 porous materials by considering air dissolved in water. *Computer Modeling in Engineering and*
556 *Sciences* 2009; **53**: 255–302.

557 [64] Gawin D, Sanavia L. Simulation of cavitation in water saturated porous media considering effects
558 of dissolved air. *Transport in Porous Media* 2010; **81**: 141–160.

559 [65] Kakogiannou E, Sanavia L, Nicot F, Darve F, Schrefler BA. A porous media finite element
560 approach for soil instability including the second-order work criterion, *Acta Geotechnica* 2016;
561 **11**(4): 805–825.

562 [66] Cao TD, Sanavia L, Schrefler BA. A thermo-hydro-mechanical model for multiphase
563 geomaterials in dynamics with application to strain localization simulation. *International Journal*
564 *for Numerical Methods in Engineering* 2016; **107**(4): 312–337.

565 [67] Sheng D, Sloan SW, Gens A, Smith DW. Finite element formulation and algorithms for
566 unsaturated soils. Part I: Theory. *International Journal for Numerical and Analytical Methods in*
567 *Geomechanics* 2003; **27**(9): 745–765.

568 [68] Cattaneo F, Della Vecchia G, Jommi C. Evaluation of numerical stress-point algorithms on
569 elastic–plastic models for unsaturated soils with hardening dependent on the degree of saturation.
570 *Computers and Geotechnics* 2014; **55**: 404–415.

571 [69] Daouadji A, Al Gali H, Darve F, Zeghloul A. Instability in Granular Materials: Experimental
572 Evidence of Diffuse Mode of Failure for Loose Sands. *Journal of Engineering Mechanics* 2010;
573 **136**(5): 575–588.

574 [70] Mokni M, Desrues J. Strain localisation measurements in undrained plane-strain biaxial tests on
575 hostun RF sand. *Mechanics of Cohesive-Frictional Materials* 1998; **4**: 419–441.

576 [71] Alesani M, Fantini S. Stability analysis of the mechanical behaviour of granular materials under
577 undrained conditions (in Italian). *Master Thesis*, Politecnico di Milano (Italy), 1998.

578 [72] Desrues J, Viggiani G. Strain localization in sand: an overview of the experimental results
579 obtained in Grenoble using stereophotogrammetry. *International Journal for Numerical and*
580 *Analytical Methods in Geomechanics* 2004; **28**: 279–321.

581 [73] Panteghini A, Lagioia R. An extended modified cam-clay yield surface for arbitrary meridional
582 and deviatoric shapes retaining full con-vexity and double homothety. *Géotechnique* 2018; **68**(7):
583 590–601.

584 [74] Panteghini A, Lagioia R. An approach for providing quasi-convexity to yield functions and a
585 generalized implicit integration scheme for isotropic constitutive models based on 2 unknowns.
586 *International Journal for Numerical and Analytical Methods in Geomechanics* 2018; **42**(6): 829–
587 855.

588 [75] di Prisco C, Imposimato S, Nova R. Sand specimen undrained mechanical response to
589 instantaneous load increments. *Proceedings of Plasticity'99, 7th International Symposium on*
590 *plasticity and its current applications*, Cancun, Mexico, 557–560, 1999.

591

592 Table 1: List of constitutive parameters.

Hyperelastic law	
$\hat{k}$	slope of the swelling isotropic compression line
a	deviatoric-volumetric elastic coupling parameter
G_0	representative elastic shear modulus
p_r	reference pressure
Yield function	
m_f	yield function shape parameter
α_f	yield function shape parameter
M_{cf}	stress obliquity for local yield locus maximum in triaxial compression
M_{ef}	stress obliquity for local yield locus minimum in triaxial extension
Plastic potential	
m_g	plastic potential shape parameter
α_g	plastic potential shape parameter
M_{cg}	stress obliquity for isochoric plastic flow in triaxial compression
M_{eg}	stress obliquity for isochoric plastic flow in triaxial extension
Hardening rule	
ρ_s	mechanical hardening of pre-consolidation pressure
ζ_s	dilatancy at failure
r_{sw}	hydraulic hardening of pre-consolidation pressure
Viscous nucleus	
γ	fluidity parameter
α	viscous nucleus shape parameter

593

594

595

596

597 Table 2: Literature experimental tests on Hostun sand used for model calibration/validation.

Test name	**Drainage**	**p'_0 [kPa]**	**e_0 [-]**	**Reference**
Triaxial compression tests				
hos011	Drained	300	0.574	Gajo and Wood (1999) [50]
hos027	Drained	200	0.578	
hosfl10	Drained	300	0.800	
hosfl11	Drained	300	0.897	
d4	Drained	300	0.945	
hosfl14	Drained	50	0.838	
hflw10	Drained	600	0.822	
batr02	Undrained	200	0.940	

batr06	Undrained	200	0.830	
alert9	Undrained	200	0.666	
400.95_1i	Drained	400	0.950	Pham Van Bang et al. (2007) [8]
CD-1	Drained	100	1.052	
CD-2	Drained	300	0.954	
CD-3	Drained	750	1.010	Daouadji et al. (2010) [69]
ICU-1	Undrained	100	1.086	
ICU-2	Undrained	300	1.060	
ICU-3	Undrained	750	1.083	
Biaxial compression test				
SHFND05	Undrained	800	0.945	Mokni and Desrues (1998) [70]
Creep tests				
T100a	Drained	100	0.950	di Prisco and Imposimato (1996) [1]
80.71_ci	Drained	80	0.710	Pham Van Bang et al. (2007) [8]
20DP13	Undrained	100	0.900	Alesani and Fantini (1998) [71]

598

599 Table 3: D_r-insensitive constitutive parameters.

Elastic law	Yield locus	Plastic potential
a=0.0	α_f=0.99	α_g=0.24
k=0.0046	m_f=1.10	m_g=1.10
p_r=1 kPa	M_{cf}=0.52	M_{cg}=1.28
	M_{ef}=0.44	M_{eg}=1.0

600

601 Table 4: D_r-dependent constitutive parameters.

Sample Density	G_0 [kPa]	ρ_s [-]	ξ_s [-]	r_{sw} [-]
Loose	14000	111	0.00	5.45
Dense	45000	2000	0.480	0.32
Limit void ratios	e_{max}	1.041	e_{min}	0.58

602

603 Table 5: Viscous parameters for loose Hostun sand (from drained creep tests).

Viscous nucleus	γ [s^{-1}]	α [-]
linear	$4 \cdot 10^{-9}$	1.0
exponential	$2 \cdot 10^{-14}$	28.90

604

605

606 Table 6: Viscous parameters for dense Hostun sand (from drained creep tests).

Viscous nucleus	γ [s^{-1}]	α [-]
linear	$1 \cdot 10^{-8}$	1.0
exponential	$2 \cdot 10^{-10}$	28.90

607

608

609 Table 7: Viscous parameters for undrained conditions (exponential viscous nucleus).

Sample density	γ [s^{-1}]	α [-]
TXU - Loose	$2 \cdot 10^{-5}$	28.90
TXU - Dense	$2 \cdot 10^{-4}$	28.90

610